Doping Strategy for Efficient and Stable Triple Cation Hybrid Perovskite Solar Cells and Module Based on Poly(3-Hexylthiophene)[P3HT] Hole Transport Layer

Narges Yaghoobi Nia[1], Enrico Lamanna[1‡], Mahmoud Zendehdel[1,2‡], Alessandro L. Palma[1], Francesca Zurlo[3],Luigi Angelo Castriotta[1], Aldo Di Carlo[1,4]**

((Optional Dedication))

1 Dr. N. Yaghoobi Nia, Dr. E. Lamanna, Dr. M. Zendehdel, Dr. A. L. Palma, Dr. L. A. Castriotta, Prof. A. Di Carlo;
CHOSE. (Centre for Hybrid and Organic Solar Energy), University of Rome ‘‘Tor Vergata’’, via del Politecnico 1, Rome 00133, Italy.

2 Dr. M. Zendehdel;
K.S.R.I (Kimia Solar Research Institute), Kimia Solar Company, Kashan, 87137-45868, Iran.

3 Dr. F. Zurlo;
Department of Chemical Science and Technologies, University of Rome Tor Vergata, Via della Ricerca Scientifica 1, 00133 Rome, Italy.

4 Prof. A. Di Carlo;
LASE - Laboratory for Advanced Solar Energy, National University of Science and Technology, NUST-MISiS, 119049 Leninskiy prosect 6. Moscow, Russia.

Corresponding Authors: Dr. N. Yaghoobi Nia & Prof. A. Di Carlo;
E-mail: YAGHOOBI.NIA@ing.uniroma2.it & E-mail: aldo.dicarlo@uniroma2.it

Keywords: ((polymeric htm, photovoltaic module, perovskite interface, thermal stability, light soaking))

As Hole Transport Layer (HTL) for perovskite solar cells (PSCs), Poly (3-Hexylthiophene) (P3HT) has been attracting a great interest due to its low-cost, thermal stability, oxygen impermeability and strong hydrophobicity. In this work, a new doping strategy has been developed for the P3HT as HTL in triple-cation/double-halide ((FA1-x-yMAxCsy)Pb(I1-xBrx)3) mesoscopic PSCs. Photovoltaic performances and stability of solar cells show remarkable enhancement using a composition of three dopants Li-TFSI, TBP and Co(III)-TFSI reaching power conversion efficiencies of 19.25% on 0.1 cm2 active area, 16.29% on 1 cm2 active area and 13.3% on a 43 cm2 active area module without using any additional absorber layer or any interlayer at the PSK/P3HT interface. The results illustrate positive effect of cobalt dopant on the band structure of perovskite/P3HT interface leading to an

improved hole extraction and a decrease of trap-assisted recombination. Non-encapsulated large area devices show promising air stability through keeping more than 80% of initial efficiency after 1500 hr in atmospheric conditions (RH~60%, r.t.), while encapsulated devices show more than 500 hr at 85 °C thermal stability (>80%) and 100 hr stability against continuous light soaking (>90%). The boosted efficiency and the improved stability make P3HT a good candidate for low-cost large-scale PSCs.

1. Introduction

In less than a decade of research, the extensive studies performed on perovskite solar cells (PSCs) led to a dramatic increase in their power conversion efficiency (PCE) exceeding now 25.2%.[1–4] This significant enhancement can be attributed to the superior properties of organo-metal halide perovskite, such as direct and tunable band-gap, high absorption coefficient, good charge carrier mobility, reasonable hole/electron diffusion lengths, solution processability, low-cost and abundant precursor materials.[5–9] In a typical mesoscopic n-i-p PSC structure, the perovskite layer is sandwiched between electron and hole transport layers (ETL and HTL, respectively).[10] Different types of scaffold ETLs have been used to fabricate high efficiency PSCs with mesoporous structure[11–13] even though TiO_2 is the most common one.[7,14] On the other hand, 2,2',7,7'-tetrakis(N,N-di-p-ethoxyphenylamine)- 9,9'-spirobifluorene (spiro-OMeTAD) is the most used HTL. It has become a worthwhile goal to find alternative Hole Transport Materials (HTMs) to replace Spiro-OMeTAD, given the high cost of spiro-OMeTAD due to a complex synthesis[15], which could hinder commercial applications,[16,17] together with thermal and chemical instability[18–20] and low charge carrier mobility.[21]

Several other compounds have been proposed as HTL, comprising inorganic material (NiO, CuSCN) and organic semiconducting polymers such as Poly(3-hexylthiophene) (P3HT) (PEDOT:PSS) and poly(triarylamine) (PTAA).[22–25] Conductive polymers have attracted a

strong interest owing to their excellent charge carrier mobility, good processability and the possibility to scale up their production.[26]Among them, PTAA[27] has shown to be very suitable for high efficient PSCs even though the high cost[28] may limit its use in real applications. Recently, many studies have been conducted on P3HT as HTL[29–31] due to its unique properties, such as high hole mobility (0.1 $cm^2V^{-1}s^{-1}$), wide band gap, good solubility, thermal stability[32] and low cost (10 times cheaper than spiro-OMeTAD).[29,33] Moreover, optical, electrical and transport properties of P3HT can be easily tuned by changing the length of the side chains,[34] the molecular weight (MW),[35] the temperature[36] and by using directional crystallization techniques.[37] In addition, several reports on the environmental stability of organic HTLs have demonstrated that poly-thiophene derivatives showed better stability than small molecules due to their oxygen impermeability and robust hydrophobicity.[38]

Very recently, Jung et al.[39] demonstrated that while a conventional use of P3HT in mesoscopic PSCs provide a reverse (forward) efficiency of 15.8% (11.7%), the addition of a Wide Band Gap (WBG) perovskite interlayer between perovskite absorber and P3HT HTL allows reducing interface recombination and improve cell efficiency above 22% without appreciable hysteresis. Even though this result is remarkable, a strong improvement of P3HT based PSCs could be achieved even without WBG interlayer, as it will be presented in our work.

To improve HTL performances, various dopants have been used such as lithium bis (trifluoromethane sulfonyl) imide salt (Li-TFSI), pyridine-based additive such as 2,6-di-tertbutylpyridine (D-TBP)[40] and 4-tert butylpyridine (TBP),[41] F4TCNQ[42] and carbon nanotubes (BCNs).[43] Accordingly, the presence of Li^+ is known to influence the doping mechanism of the HTM[44,45] as well as the mobility of charges. Electrochemical Impedance Spectroscopy(EIS) results evidenced that PSCs without Li-TFSI in HTL show an additional

resistive element that is most likely related to the transport resistance in the HTL.[46] On the other hand, the addition of TBP increases the hole selectivity of the HTL/perovskite interface[41], improves the uniformity of the HTL and avoids accumulation of Li salt.[47]

These doping strategies have been mainly developed for spiro-OMeTAD and may not be optimal for other HTLs. By applying the doping strategies the non-radiative recombination losses of PSCs can be mitigated. For example, Tavakoli et al. have been shown the potential of adamantylammonium iodide as the HTL dopant in order to improve the overall efficiency and stability of single and double cation perovskite solar cells, reaching 22% PCE and more than 500 hr stability.[48] Owing to the higher HOMO level of P3HT (-4.8 eV) with respect to spiro-OMeTAD (-5.1 eV), PSCs employing Li-doped P3HT have not been able to achieve high PCEs due to significant loss of the open-circuit voltage (V_{OC}).[49] Therefore, a dopant that has the capability to lower the Work-function of the P3HT is also requested.

Cobalt inorganic complexes,[50–54] induce, through an oxidative doping,[55]a lowering of Fermi level of the HTL resulting in an increase of V_{OC}.[56] In addition, the Co-doped devices showed an improved stability under light.[49] Jung et al. successfully used a Cobalt complex as a dopant of P3HT in a $MAPbI_3$-based flexible solar cells with PCE of 11.8%.[49] This Co complex led to an enhancement of the P3HT conductivity and to a downward shift of the energy levels.

In our previous works, we evaluated the relationship between P3HT molecular weight (MW) and the PCE of PSCs.[31,57] The results showed that by increasing the P3HT's MW the PCE improve mainly due to an enhancement in electron lifetime. Under these circumstances, by using Li-TFSI and TBP and the crystal engineering approach[58,59] for fabrication of $MAPbI_3$ based PSCs under ambient condition, the PCE of the PSCs containing 124 kDa P3HT as

HTM layer was improved up to 16 % for small area devices (active area 0.1 cm^2) and 11.2 % stabilized efficiency for module (Active area 10.1 cm^2).[58]

In this work, a new doping strategy for the P3HT has been investigated. We consider the mixing Li-TFSI, TBP and FK209 Co(III)-TFSI as P3HT dopant in a mixed cation mesoscopic PSC to improve the photovoltaic performance and thermal stability of the fabricated devices. Mixed cation perovskites having methylammmonium (MA), formamidinium (FA), and Cs as cations with I and Br as halide tend to exhibit high efficiency and robust stability against light and heat stress.[60]At the same time, however, mixed cation PSCs still suffer from degradation of the fill factor, which can stem from decreased conductivity of degraded organic molecular HTMs, such as spiro-OMeTAD.[61,62] Indeed, replacement of molecular HTMs with thermally stable polymers like P3HT, not only could be favorable for up-scaling, but also could improve the life span of the devices. Following our previous investigation[31] we focus on P3HT with a MW of 124 kDa, employing our new doping strategy for the fabrication of cells and modules with different size, as shown in **Figure 1**.

a)

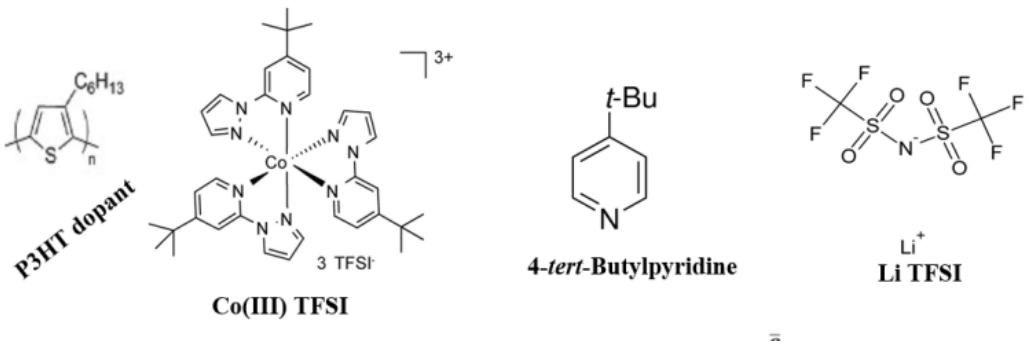

b)

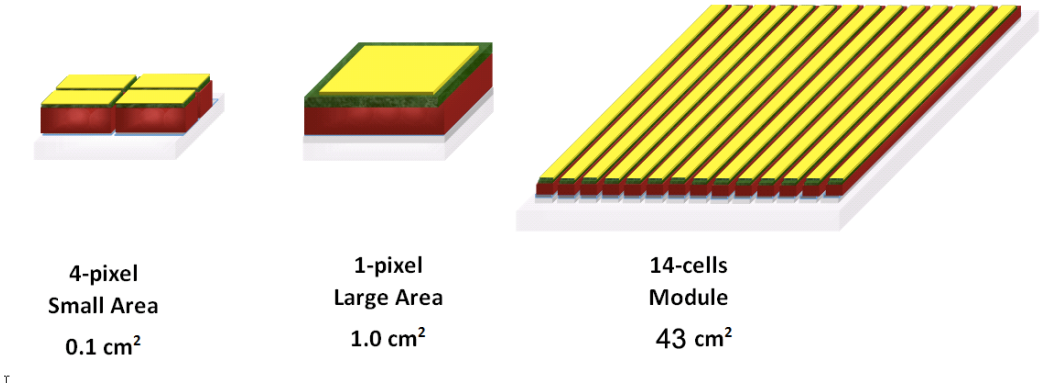

c)

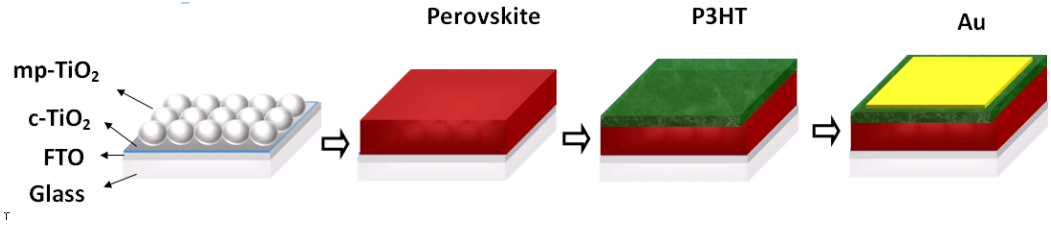

Figure 1. a) Chemical structure of the P3HT and of its dopants used in this work. b) Schematic figures of the fabricated PSCs and modules using P3HT as HTL. The active area of the small area devices, large area devices and modules are 0.1 cm^2, 1.0 cm^2 and 43 cm^2, respectively. c) Schematic figure that illustrate the deposition steps.

2. Results and Discussion

2.1. Doping Effect on P3HT Thin Film

The effect of different dopants on the performance of the P3HT thin film has been evaluated by spectroscopic method. UV-VIS absorbance spectra of the P3HT layers with different dopant composition deposited on the triple cation perovskite layer and on the FTO substrate are shown in **Figure 2**(a), while normalized absorbance spectra of P3HT on FTO in Figure 2(b). The well-defined onset of absorbance spectra around 730 nm clearly show the formation of the perovskite phase with a full surface coverage.[63] With respect to perovskite layers, samples covered by P3HT show higher absorbance values in the range of 500-650 nm, which could be attributed to the addition of P3HT absorption to the perovskite one (see dashed lines in Figure 2(a)).[31] In particular, the P3HT layer with cobalt complex dopant in addition to Li-salt and TBP shows higher absorbance in this region with respect to the other P3HT layers. The absorbance spectrum of the non-doped P3HT layer shows a broad peak at 514 nm

containing two shoulders at 553 nm and 603 nm (see Figure 2(b)). The absorbance peak at 514 nm provides information on the degree of conjugation of the P3HT chains, whereas the shoulders provide information on the degree of interchain order.[64–66] By adding dopants to P3HT we can see a clear variation in the absorbance spectra. The P3HT layer containing Li-salt and TBP dopants shows a broad peak at 553 nm and a low marked shoulder at around 600 nm. By adding the cobalt complex, a clear red shift of P3HT absorbance and enhancement of the shoulders can be observed. These results show that the dopants have positive effects on conjugation degree of the thiophene chains, with a consequent decrease of the band gap, and on the degree of interchain order.[64] Furthermore, in order to determine the direct band gap energy of the P3HT thin films, diffuse reflectance spectroscopy (DRS) has been used as a useful characterization tool for a wide variety of substrates.[67–70] Accordingly, DRS spectra of the P3HT thin films at FTO substrate have been collected and direct-allowed band-gap values have been extracted from Kubelka-Munk function.[67] As presented in **Figure S1**, direct band gap of P3HT layer is clearly decreased by dopping strategy. Band structure of the P3HT layer at both doped and no-doped states has been evaluated through cyclic voltametery analysis of diode structure (see Figure S1(b)). Accordingly, in the diode structure the P3HT layer (doped and no-dped) has been sandwiched between FTO and Au and the electrochemical propoerties has been studed under dark conditions. The HOMO level of the P3HT layer has been changed from –4.95 eV to –5.24 eV by addition of the dopants.

Photoluminescence (PL) curves of the perovskite-based layers are presented in Figure 2(c). The PL emission peak at 759 nm quenched significantly in sample with PSK/P3HT with respect to the one with only PSK. Reduced PL intensity is mainly related to better charge extraction from the perovskite layer and this is well consistent with interfacial morphology.[58,71] We should point out that P3HT doped also with Cobalt complex shows a higher PL quenching with respect to the Cobalt-free sample.

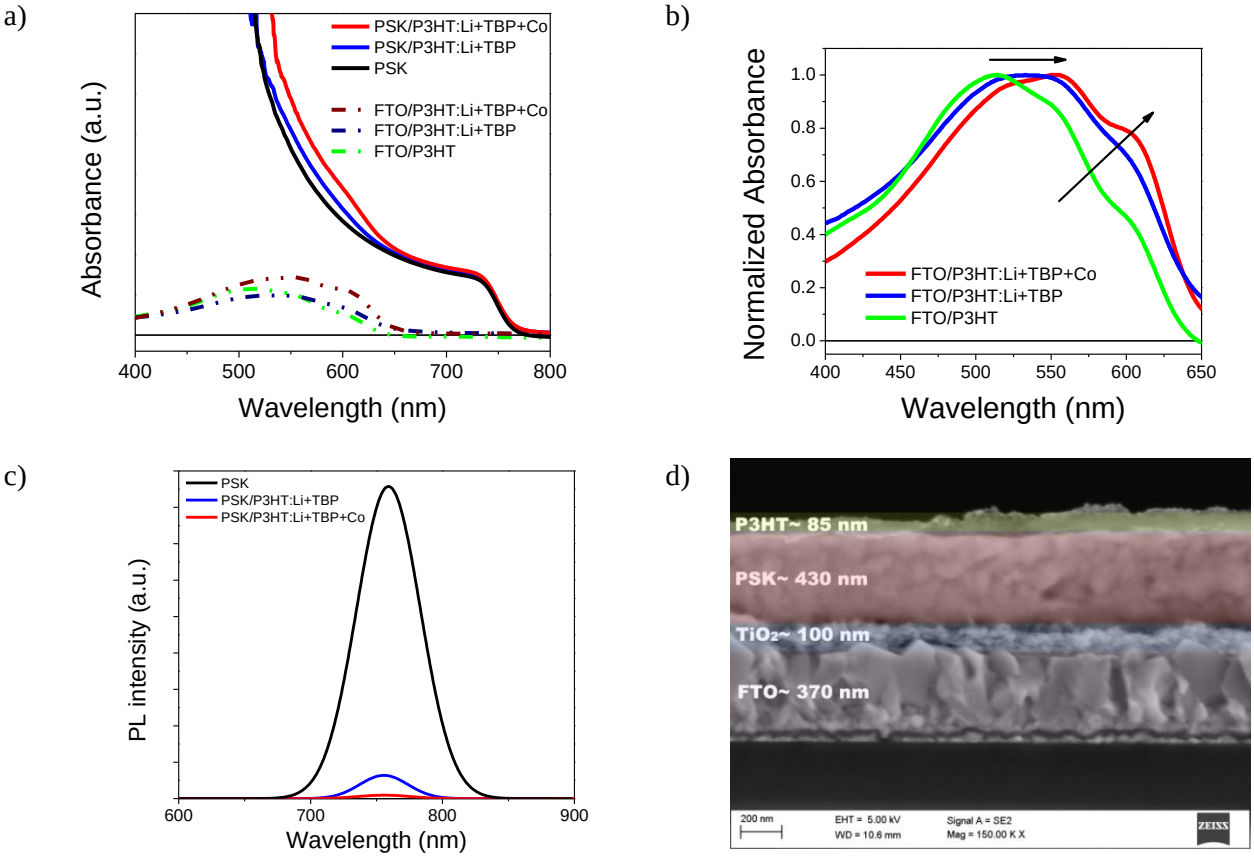

Figure 2. a) UV-Vis absorbance spectra of the P3HT with different composition of dopants on the perovskite (PSK) and on FTO substrate. b) Normalized absorbance of the P3HT on FTO in the range of 400-650 nm. c) Photoluminescence spectra of the perovskite and P3HT coated perovskite with different composition of HTM dopants. d) cross section SEM image from the thin film consist of FTO/mp-TiO_2/PSK/P3HT:Li+TBP+Co.

PSCs with a FTO/mp-TiO_2/PSK/P3HT/Au stack (without c-TiO_2) have been fabricated by using P3HT doped with Li-salt, TBP and Cobalt complex. The cross section SEM image of the stack (without Au) is presented in Figure 2(e). The thicknesses of the FTO, mp-TiO_2, PSK and P3HT layers are ~360 nm, ~100 nm, ~430 nm and ~70 nm, respectively.

2.2. Photovoltaic Performances

PSCs' photovoltaic performances have been evaluated by JV measurement under 1-sun AM1.5G solar simulator and the statistic results are shown in **Figure 3**. Full doped (Li+TBP+Co) small area devices (0.1 cm^2 as active area) demonstrate a maximum power conversion efficiency of 19.25 %, with an average of 18.55 ±0.44 % for all the batch of

devices, and a stabilized PCE of 18.4 % (**Figure 4**(a)); at the same time, the devices without cobalt dopant reached a maximum PCE value of 15.62 % with an average of 14.23 ±0.72 %.

The Co-doped large area devices (1.0 cm^2 as active area) show a PCE statistical distribution in the range of 15.55-16.29 % with average of 15.93±0.30 %, and a stabilized PCE of 16.10 % (Figure 4(a)). Based on our knowledge, the presented PCEs are the highest reported efficiencies for the mesoscopic perovskite using P3HT as HTM without any interlayer at the PSK/P3HT interface. The full-doped PSCs show promising high photovoltage and photocurrent with around 70% fill factor and highly reproducible results. The J-V curve of the champion small area device at 1-sun is presented in Figure 4(b) by sweeping the voltage in both forward and reverse scan directions and the corresponding photovoltaic parameters are showed in **Table 1**. The J-V curves show a low hysteresis with a hysteresis index of 0.042.[72] The EQE curve of the champion device is also presented in **Figure S2**.

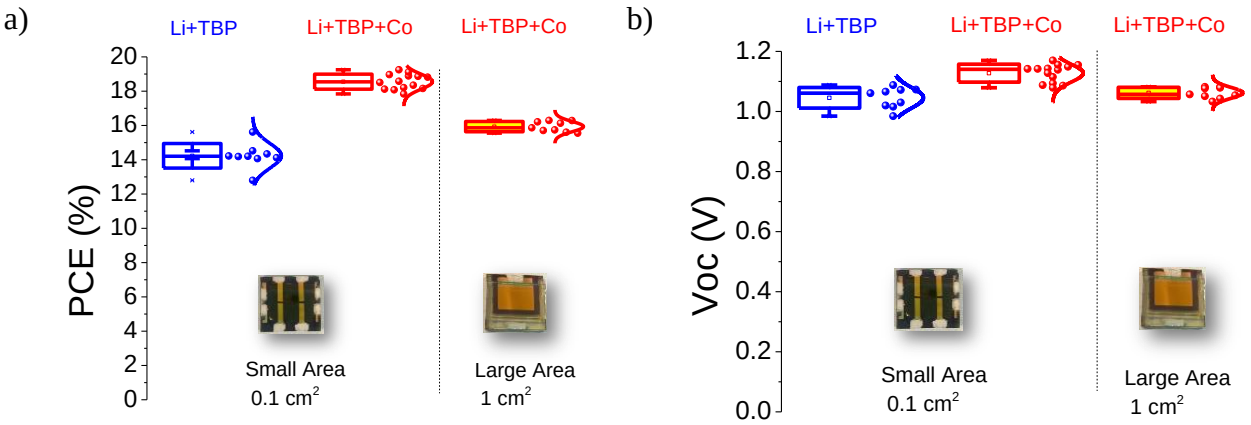

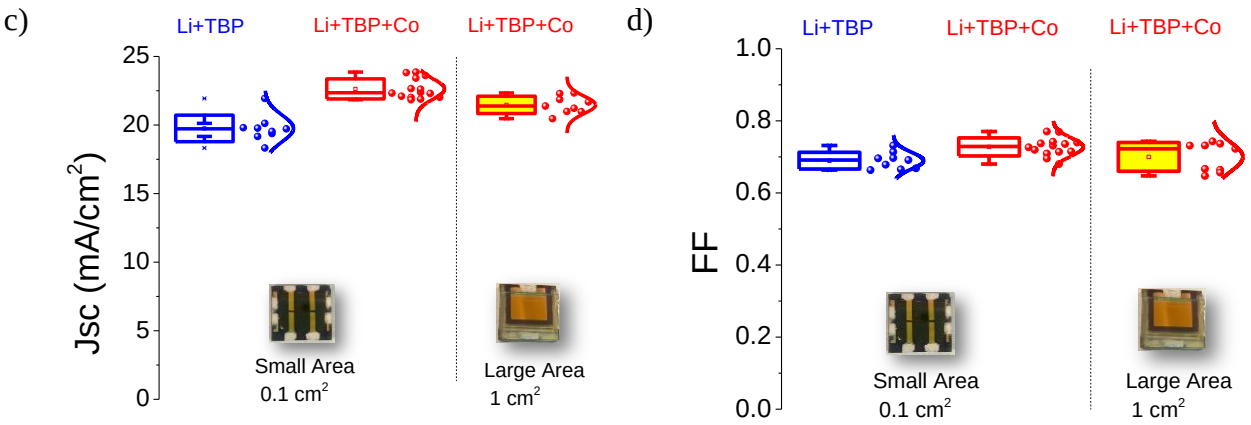

Figure 3. Statistical photovoltaic parameters of the small area and large area PSCs containing P3HT as HTM with different dopant mixture. a) PCE, b) Voc, c) Jsc and d) fill factor.

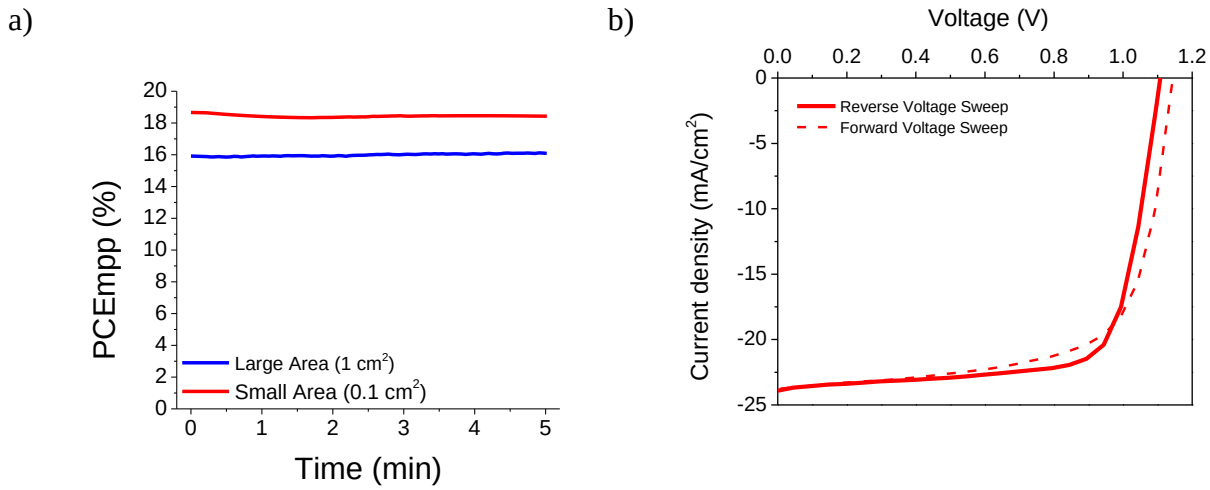

Figure 4. a) Maximum power point tracking of selected small area and large area PSCs. b) J-V plot of the champion small area device with sweeping of the voltage in both forward and reverse scans.

Table 1. Photovoltaic parameters of the best performance small area PSC in both forward and reverse voltage sweep.

Voltage sweep	Voc (V)	Jsc (mA/cm^2)	FF	PCE (%)
Reverse	1.09	23.86	0.737	19.25
Forward	1.14	23.82	0.680	18.51

2.3. Electrochemical Properties

To investigate the electrochemical properties of PSC interfaces with or without cobalt complex doping of the P3HT layer, Electrochemical Impedance Spectrometry (EIS) of PSCs has been performed under dark conditions with a bias voltage range between 0.6 V and 1.0 V. As shown in **Figure 5**(a), Nyquist plots composed of two irregular semicircles, including the very small one at high frequency and the large one at low frequency (equivalent circuit is the figure inset). R_s is mainly related to the resistance of the FTO substrate.[73,74] The first semicircle is attributed to the hole transport resistance (R_1) at the HTL/perovskite interface. The second semicircle in the low frequency range is associated to the recombination resistance (R_2) at the HTL/perovskite interface.[31,58,75] The fitted values of the resistive elements are plotted in **Figure S3**. Both devices show almost the same series resistance, however the cobalt complex doped PSC shows markedly higher hole extraction and lower charge recombination compared to the cobalt-free layer. The EIS results clearly show the positive effect of the cobalt complex dopant on the P3HT/perovskite interface, which is in good agreement with the higher photovoltaic performance of this device with respect to the cobalt free PSCs. The cobalt complex can effectively intercalate between the thiophene backbones and led to dramatically change the HOMO level of P3HT to more negative values enhancing hole extraction and decreasing the charge recombination at the perovskite/P3HT interface.[50]

Electrochemical properties of the P3HT-based PSCs with different compositions of HTM dopants have also been investigated using Cyclic Voltametery (CV) in dark condition for a bias voltage between -1.5 and 1.5 V. The Tafel plots of the CV analysis are shown in Figure 5(b). The comparison between Tafel plots evidences that, independently from the doping strategy, devices do not show any hysteresis between anodic and cathodic cycles, while the leakage current of the cobalt-free sample is lower than the one with cobalt doping. Dark JV is

also a powerful tool to analyse the recombination process in the solar cell. By applying a bias (dark condition), the current flowing through the device could be expressed as,[76]

$$I = I_{01}e^{\frac{V-IR_S}{2kt/q}} + I_{02}e^{\frac{V-IR_S}{kt/q}} + \frac{V - IR_S}{R_{SH}} \quad (1)$$

Where, I_{01} and I_{02} are diode saturation currents, R_S and R_{SH} are the series and shunt resistance of the device, respectively. According to Equation 1, and considering the experimental results shown in Figure 5(c), the IV characteristics can be divided into 4 bias regions: 1) $V < V_1$, dark current will be related to the shunt resistance; 2) $V_1<V<V_2$, the dominant term is the first exponential of Equation 1 that is related to the recombination in the depletion zone; $V_2<V<V_3$, the dominant term is the second exponential of Equation 1 that is related to trap assisted and radiative recombination; $V>V_3$ dark current is limited by the series resistance and will saturate.

In our devices V_1-V_2 voltage range reduces when cobalt is added to the TBP+Li doped P3HT. This clearly shows a positive effect of the cobalt complex at the perovskite/HTL interface, enhancing the rate of hole extraction and reducing the direct recombination, which is the third term on the right-hand side of equation (1).

At V_2, when the bias voltage exceeded the kink point corresponding to Trap-Filled Limit voltage (V_{TFL}),[77,78] the current quickly increased, indicating that the trap-states were completely filled. The dark JV results are in good agreement with EIS, demonstrating that the photovoltaic improvement by cobalt doping in the P3HT via notably decrease in charge recombination.

In order to investigate the effect of dopants in the P3HT layer without considering the perovskite/P3HT interface, diode structure of P3HT in both no Co-doped and Co-doped states has been realized by sandwich the polymer film between FTO and Au electrodes (**Figure S4**).

In this diode structure, any electrode offers an ohmic response to the polymer/metal interface and the injected carriers from electrode leads to formation a space charge region consisting of a large number of injected carriers and equilibrium free carriers into the polymer layer. Because of low carrier mobility, more charges are injected before transferring of injected carriers from one to the other electrode. When an external electric field is applied, further charges will injected from low-barrier electrode to the P3HT, and an equilibrium stage is reached when injected carriers are comparable to the free carriers concentration. Thus at this stage, the flow of current could be referred as space charge–limited current.[79] JV curves of P3HT based diodes (P3HT:Li+TBP layer compared to P3HT:Li+TBP+Co film sandwiched between FTO and Au electrodes) under dark condition have been presented in Figure S4(a). The applied bias potential sweep from -1.2 V to +1.2 V with 50 mV/s as scan rate. In order to evaluate the Space Charge-Limited Current behavior, the curves has been shown in logarithmic scale of both J and V (Figure S4(b)). Higher slop values of the Co doped P3HT shows the positive influence of the cobalt complex for improving of the carrier mobility of P3HT thin film.[79] This carrier mobility enhancement by cobalt complex could be attributed to formation of polarons (radical ions) or bipolarons (dication or dianions) in the P3HT layer due to oxidation/reduction process.[80] The movement of such charge carriers along polymer chains can produce more conductivity.

Transient Photocurrent (TPC) and Transient Photovoltage (TPV) analysis have been also performed for PSCs with the different composition of dopants in P3HT. The extracted charge versus Jsc are evaluated from TPC analysis[81,82] and plotted in Figure 5(c). These results are in good agreement with EIS data showing a marked improvement of hole extraction in Co doped P3HT with respect to those without Co. In addition, the recombination time, evaluated from TPV[82] (Figure 5 (d)), is larger in Co-doped P3HT with respect to the one without Co doping. Considering that the combination of high carrier mobility together with high diffusion

length of PSCs limits charge recombination at the interfaces between perovskite layer and HTL, the cobalt complex seems to reduce the amount of recombination centers, as also confirmed by EIS and dark JV results.

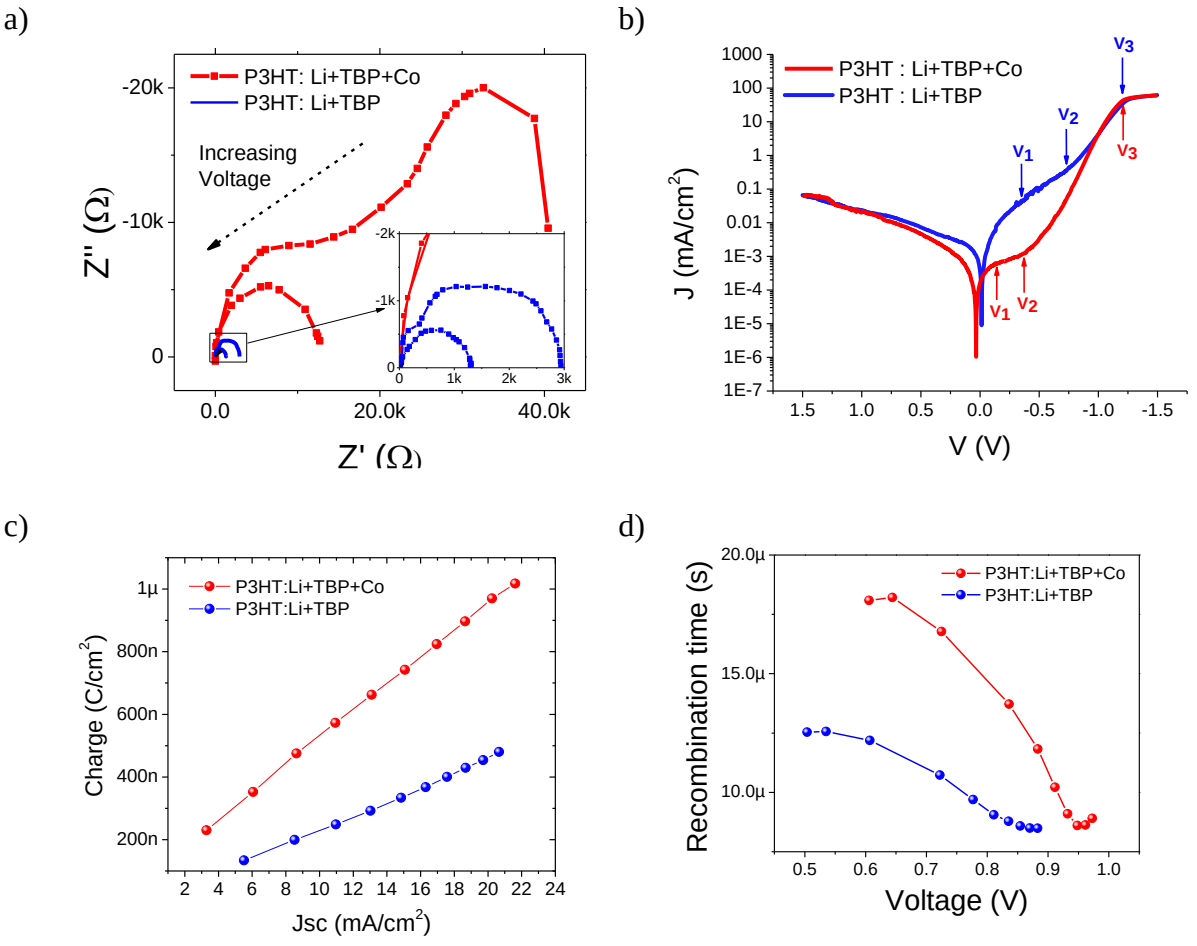

Figure 5. a) Nyquist plot from EIS results and equivalent fitting circuit of the PSCs containing P3HT as HTM and different composition of dopants. b) Tafel plots of the devices with different compositions of P3HT dopants evaluated from Cyclic Voltametery Analysis. c) Charge Extraction curves of the PSCs obtained from Transient Photocurrent Fall/Rise Analysis. d) Recombination time vs voltage, evaluated from Transient Photovoltage Decay Analysis of the PSCs.

2.4. Stability Results

Life span analysis of the fabricated PSCs (large area device structures with 1.0 cm^2 active area) containing (Li+TBP+Co) or (Li+TBP) dopant combination has been evaluated by shelf life analysis (no-sealed devices), thermal stress and constant 1-sun light soaking accelerated test (encapsulated devices). The tracking of devices' PCE is reported in **Figure 6**.

Atmospheric shelf life span analysis is performed on non-encapsulated PSCs kept in ambient condition at a temperature of ~25 °C and a Relative Humidity of ~60%. The results show that the Co based devices retain more than 80% of their initial PCEs after 1500 hr. Furthermore, thermal stability analysis of encapsulated PSCs is performed by keeping the devices at 85 °C in an oven out of glove box. The results demonstrate that Co-doped devices retain 80% of their initial PCE after thermal stress for more than 500 hr. The same encapsulated large area devices have been tested against light soaking (Figure 6 (c)). The light soaking results also show that Co based PSC could keep about 90% of initial efficiency after 100 hr continuous irradiation. The accelerated stability results of the full-doped devices show amazing enhancement also compare to control P3HT-based device (without wide-bandgap interlayer) of recently published high efficiency P3HT-based wide-bandgap interlayer perovskite.[39] These promising shelf-life, thermal and light stability could be attributed to intrinsic characteristics of P3HT as oxygen impermeability and hydrophobicity[38] and to the high stability of triple cation perovskite in addition to better interfacial contact between perovskite and the HTM which led to facilitating hole transfer at the interface.[39] The Co-complex at the perovskite/HTL interface can suppress trap states,[83] so that there is less degradation of the device with the Co-complex dopant, which may contribute to the enhancement of interfacial polarity compatibility.[83] Indeed, our life span analyses show the promising enhancement of the P3HT-based PSCs by using Li+TBP+Co doping strategy in comparison with other P3HT dopants such as F4TCNQ and single walled carbon nanotubes (SWCNTs).[42,84]

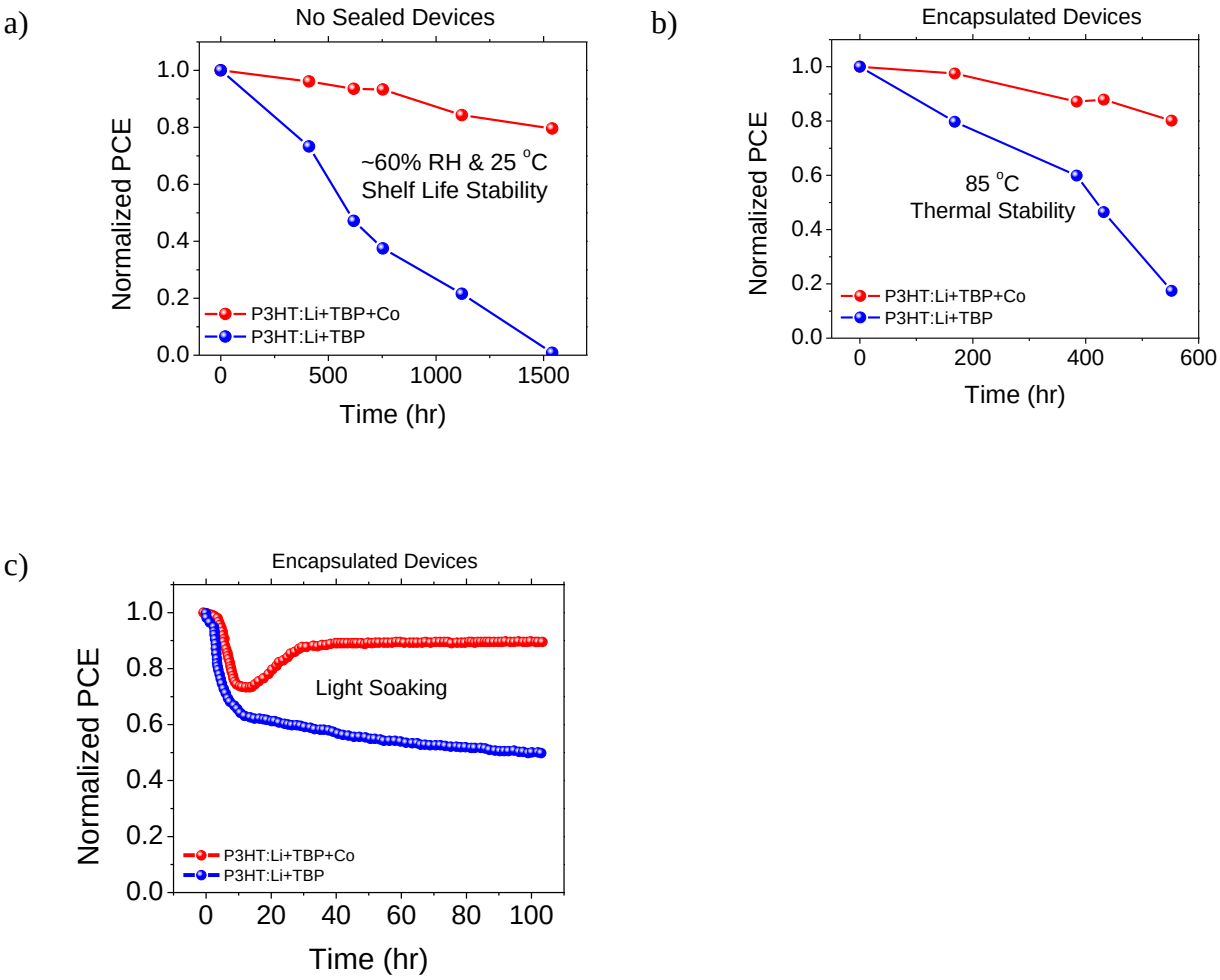

Figure 6. a) Shelf Life stability analysis (under atmospheric conditions) of not sealed PSCs, b) thermal stability of encapsulated PSCs, and c) light stability graphs of the PSCs under constant 1-sun light soaking accelerated test. Comparison between two P3HT's dopants composite is shown.

2.5. Up-scaling to Perovskite Solar Module

To prove the up-scaling capability of the P3HT based PSCs, we realized a 10 cm x10 cm perovskite solar module with an active area dimension of 43.0 cm^2, using triple cation perovskite as active layer and P3HT (fully doped with Li-TFSI, TBP and Cobalt complex) as HTL. The photovoltaic parameters of the fabricated module evaluated under AM1.5G simulated irradiation are presented in **Figure 7** and **Table 2**. The structure of the module consists of 14 separate series-connected cells. Open-circuit voltage and short-circuit current density of the module are 15.1 V and 17.7 mA/cm^2, respectively, while the module fill factor

is 69.8%. Due to series connection of the 14 cells we can calculate the power conversion efficiency under 1-sun illumination through following formula;

$$PCE = ({}^{Voc}/_{Nsc}) \times Jsc \times FF \quad (2)$$

which Nsc show the number of series connected cells. The module can generate 474 mW electrical power output at maximum power point, with a PCE of 13.3%. Owing to control the reproducibility, 8 batches of modules with same dimension have been realized and the statistic results have been shown good reproducibility with PCE mean of 12.9 ±0.67 %.

a)

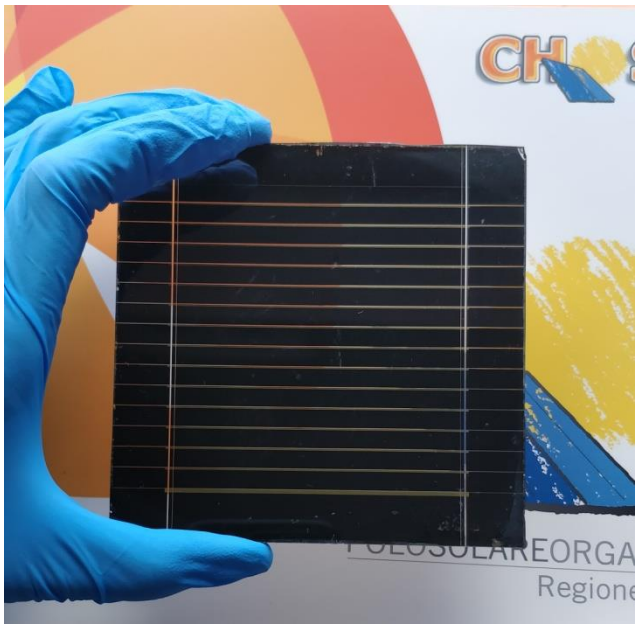

b)

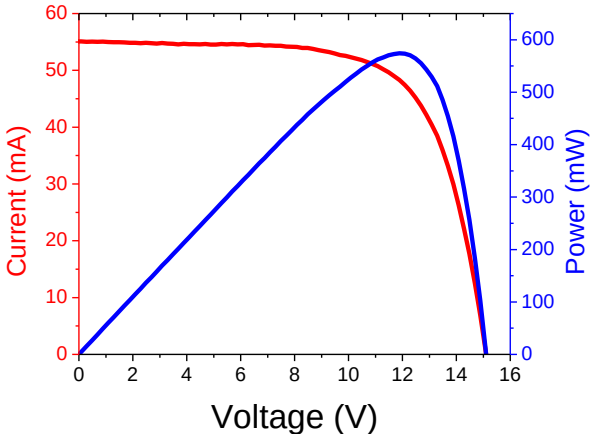

Figure 7. Picture of the fabricated module (a). JV curve of the module under AM1.5G simulated 1-sun showing Pmax of 193 mW (b).

Table 2. PV characteristics of the full-doped P3HT-based perovskite solar module.

Module type	14 series cells
Active Area	43 cm^2
Pmax	474 mW
Vmp	11.9 V
Imp	48.3 mA
Voc	15.1 V
Jsc	17.7 mA/cm^2
FF	69.8 %
PCE	13.3 %

3. Conclusion

In this work, we successfully used a new doping strategy for the P3HT as HTM of triple-cation/double-halide hybrid perovskite ($(FA_{1-x-y}MA_xCs_y)Pb(I_{1-x}Br_x)_3$) mesoscopic solar cells, by mixing Li-TFSI, TBP and FK209 Co(III)-TFSI. The fabricated devices using the three HTM dopants (Li+TBP+Co) show remarkable enhancement of the photovoltaic performance and device stability, reaching a PCE of 19.25%, 16.29% and 13.3% for small area (0.1 cm^2), large area (1.0 cm^2) and perovskite solar module (43 cm^2 active area), respectively. Non-encapsulated devices show a promising (>1500 hr) shelf life stability in atmospheric conditions (RH~60%, r.t.). Furthermore, encapsulated devices show more than 500 hr thermal stability at 85 °C and more than 100 hr light stability against continues 1-sun irradiation. Results show that cobalt dopant can positively affect the perovskite/P3HT interface leading to an enhancement of hole extraction and a decrease of trap-assisted recombination phenomena. The dopant mixture can also positively enhance charge carrier mobility of the P3HT layer through formation of polaron or bipolaron charge carriers along polymer chains.

4. Experimental Section

Device fabrication: A raster scanning laser ($Nd:YVO_4$ pulsed at 30 kHz average outputpower P=10 W) was used to etch the FTO/glass substrates (Pilkington, 8Ωcm^{-1}, 25mm x 25mm). The patterned substrates were cleaned in anultrasonic bath, using detergent with de-ionized water, and 2-propanol, 5 minutes for each step. A compact TiO_2 (c-TiO_2) layer was deposited onto the patterned FTO by spray pyrolysis deposition using a previously reported procedure.[58] Briefly, temperature of the substrate was fixed at 450 °C, the distance between substrate and the autograph (tilted about 45° respect tothe substrate) was fixed to 20 cm. Around 15 successive spray cycles were made to reach a final thickness of 50 nm. Precursor

spray solutionwas consist of 0.16 M Disopropoxytitaniumbis(acetylacetonate) (TAA) and 0.4 M Acetylacetone (ACAC) in ethanol. Patterning of the c-TiO_2 was achieved using a screen printed metal mask which was removed afterthe c-TiO_2 deposition using an acidic solution, de-ionized water and ethanol. A nano-crystalline mesoporous TiO_2 layer (18NR-Tpaste, Dyesol), diluted with ethanol, with w/w ratio of 1:6, was spin coated onto the c-TiO_2 surface and sintered using annealing program from roomtemperature to 120 °C for 5 min and remain 5 min, 120 °C to 325 °C for15 min and stay 5 min, 325 °C to 375 °C for 5 min and stay 5 min, 375 °C to 480 °C for 5 min and remain 30 min. Then Litsalt treatment was performed on the the mesoporous layer by deposition of solution of Bis(trifluoromethane)sulfonimide lithium salt in acetonitrile (34.8 mM) via spin coating at 3000 r.p.m for 10 second and another sintering step same as was mentioned above for mesopouors layer and kept at 150°C , then immediately were transferred to the glove box to not absorb any water on the surface before perovskite deposition. Then the perovskite layer was deposited on the scaffold layer. The perovskite solution was made by mixing the solutions of $FAPbI_3$ (1.47 M) and $MAPbBr_3$ (0.18 M) precursor complexes in 1 ml of mixed DMF/DMSO solvent. Subsequently, 0.05 CSI solution was added to the mixed solution. Stock solution of CsI made by dissolving the 389.71 mg CsI powder in 1 ml DMSO.

The perovskite solution was spin coated in a two-step program, for 10 sec at 1000 r.p.m with a ramp of 200 r.p.m and 6000 r.p.m. with a ramp of 2000 r.p.m for 20 sec, respectively. During the second step, chlorobenzene was poured on the spinning substrate to form the perovskite. Then the substrates were annealed at 100 ºC for 60 min.

0.15 mM of P3HT 124 MW solut ion in chlorobenzene doped with LiTFSI/ TBP/FK209 Co(III)-TFSI (20:78:2 mol%) was deposited by spin coating at 6000 for 60 second on top of the perovskite layer. Finally 100 nm gold deposited on the substrate in a vacuum metal evaporator system.

Diode Fabrication: In order to fabricate the diode structure, 0.15 mM of P3HT 124 MW solution in chlorobenzene doped with LiTFSI/ TBP/FK209 Co(III)-TFSI (20:78:2 mol%) and no Co-doped, was deposited by spin coating at 6000 for 60 second on top of a patterned FTO layer and transferred to metal evaporator for deposition of Au back contact.

Module Fabrication: In order to produce Perovskite Solar Modules, we adopted the P1-P2-P3 patterning procedure.[85] FTO substrates were washed in the same way as small area ones, then the P1 process was realized by means of a Nd:YVO_4 ns laser (λ = 1064 nm, Fluence = 11.5 J/cm^2) to insulate the FTO photoanodes of neighboring cells. Afterwards, the substrates were kept on a hot plate, reaching 460 °C in 40 min and the solution for spray (the same for small area) was deposited by spray pyrolisys. We deposited a blocking layer with a thickness of 50 nm.

Mesopouros deposition: TiO_2 paste was diluated by 1:6 w/w ratio (TiO_2 paste: anhydrous Ethanol) and deposited for 20 second at 4000 r.p.m with a ramp of 2000 r.p.m, then substrate were annelid using same program mentioned in the small area. Then Li-salt treatment was performed on the the mesoporous layer by deposition of solution of Bis(trifluoromethane)sulfonimide lithium salt in acetonitrile (34.8 mM) via spin coating at 3000 r.p.m for 10 second and another sintering step same as was mentioned above for mesopouors layer and kept at 150°C, then immediately were transferred to the glove box before perovskite deposition to not absorb any water on the surface.

Deposition: Firstly perovskite solution deposited on the substrate and immediately start the spin Step1000 rpm, 10 s, 200 rpm/s, and second step:4000 rpm, 20 s, 2000 rpm/s, finally in the last second step, chlorobenzene was spin cast on the substrate to form the final perovskite, annealed at 100 for 1 hour. P3HT solution was spinned on the perovskite layer by spin coating at 4000 for 30 second, then 100 nm gold deposited on the substrate. After the deposition of Perovskite and P3HT layers, the P2 patterning process was applied to remove the ETM-Perovskite-HTM stack from the underneath FTO, in order to realize vertical

contacts between the latter and the subsequently deposited electrode. We operated the P2 step by means of a Nd:YVO_4 ns laser (λ = 532 nm, Fluence = 157mJ/cm^2). Finally, after the gold evaporation, the P3 laser patterning step was realized to insulate the counter-electrodes of the single cells, employing a Nd:YVO_4 ns laser (λ = 532 nm, Fluence = 70mJ/cm^2).

Device measurement and instruments: Masked devices were tested under a solar simulator (ABET Sun 2000, class A) at AM1.5G and 100 mW cm^{-2} illumination conditions calibrated with a certified reference Si Cell (RERA Solutions RR-1002). Incident power was measured with a Skye SKS 1110 sensor. Microstructural investigation of cell cross section was performed by using a field emission scanning electron microscope (FE-SEM, SUPRA™ 35, Carl Zeiss SMT, Oberkochen, Germany). IPCE was measured with a commercial apparatus (Arkeo-Ariadne, Cicci Research s.r.l.) based on a 300 Watts Xenon lamp and able to acquire spectrum from 300 to 1100 nm with 2 nm of resolution. The absorbance and Diffuse Reflectance spectroscopy analysis were measured with a BLACK-Comet UV-VIS Spectrometer. Dark JV measurement from fabricated PSCs and diode structures was done using cyclic Voltammetery module of AUTOLAB potentiostate instrument. Electrochemical impedance spectroscopy was done by AUTOLAB. TPV TPC was measured with a commercial apparatus (Arkeo, Cicci Research s.r.l.) based on a high speed Waveform Generator that drives a high speed LED (5000 Kelvin).

Supporting Information

Supporting Information is available from the Wiley Online Library or from the author.

Acknowledgements

E.L. and M.Z. contributed equally to this work. The CHOSE team acknowledges the "Accordo di Programma MiSE-ENEA sulla Ricerca di Sistema Elettrico Piano Annuale di Realizzazione 2015" and the European Union's Horizon 2020 Framework Program for funding Research and Innovation under Grant agreement no. 764047 (ESPRESSO) for funding. ADC gratefully acknowledges the financial support from the Ministry of Education and Science of the Russian Federation in the framework of Increase Competitiveness Program of NUST «MISiS» (№ K2-2019-13).

Conflict of Interest

The authors declare no conflict of interest.

Keywords
light soaking, perovskite interface, photovoltaic module, polymeric htm, thermal stability

Received: August 8, 2019
Revised: September 19, 2019
Published online:

References

[1] NREL, "Best Research-Cell Efficiencies," can be found under https://www.nrel.gov/pv/assets/pdfs/pv-efficiency-chart.20190103.pdf, accessed at September 2019.

[2] A. Kojima, K. Teshima, Y. Shirai, T. Miyasaka, *J. Am. Chem. Soc.* **2009**, *131*, 6050.

[3] H.-S. Kim, C.-R. Lee, J.-H. Im, K.-B. Lee, T. Moehl, A. Marchioro, S.-J. Moon, R. Humphry-Baker, J.-H. Yum, J. E. Moser, M. Grätzel, N.-G. Park, *Sci. Rep.* **2012**, *2*, 591.

[4] P. Meredith, A. Armin, *Nat. Commun.* **2018**, *9*, 5261.

[5] A. R. Bin Mohd Yusoff, P. Gao, M. K. Nazeeruddin, *Coord. Chem. Rev.* **2018**, *373*, 258.

[6] S. Il Seok, M. Grätzel, N.-G. Park, *Small* **2018**, *14*, 1704177.

[7] M. I. H. Ansari, A. Qurashi, M. K. Nazeeruddin, *J. Photochem. Photobiol. C Photochem. Rev.* **2018**, *35*, 1.

[8] M. Yaghubinia, Majid Ebnali, Mahmoud Zendehdel, in *PHOTOPTICS*, IEEE, Piscataway, NJ **2016**, pp. 1–3.

[9] L. Salamandra, N. Yaghoobi Nia, M. Di Natali, C. Fazolo, S. Maiello, L. La Notte, G. Susanna, A. Pizzoleo, F. Matteocci, L. Cinà, L. Mattiello, F. Brunetti, A. Di Carlo, A. Reale, *Org. Electron.* **2019**, *69*, 220.

[10] Z. Song, S. C. Watthage, A. B. Phillips, M. J. Heben, *J. Photonics Energy* **2016**, *6*, 022001.

[11] M. K. Sardashti, M. Zendehdel, N. Yaghoobi Nia, D. Karimian, M. Sheikhi, *ChemSusChem* **2017**, *10*, 3773.

[12] A. Matas Adams, J. M. Marin-Beloqui, G. Stoica, E. Palomares, *J. Mater. Chem. A* **2015**, *3*, 22154.

[13] M. Ye, X. Liu, J. Iocozzia, X. Liu, Z. Lin, Springer, Cham, **2016**, pp. 1–39.

[14] M. F. Mohamad Noh, C. H. Teh, R. Daik, E. L. Lim, C. C. Yap, M. A. Ibrahim, N. Ahmad Ludin, A. R. bin Mohd Yusoff, J. Jang, M. A. Mat Teridi, *J. Mater. Chem. C* **2018**, *6*, 682.

[15] Z. Li, J. Chen, H. Li, Q. Zhang, Z. Chen, X. Zheng, G. Fang, H. wang, Y. Hao, *RSC Adv.* **2017**, *7*, 41903.

[16] A. Abate, J.-P. Correa-Baena, M. Saliba, M. S. Su'ait, F. Bella, *Chem. - A Eur. J.* **2018**, *24*, 3083.

[17] Y. Rong, Y. Hu, A. Mei, H. Tan, M. I. Saidaminov, S. Il Seok, M. D. McGehee, E. H. Sargent, H. Han, *Science* **2018**, *361*, eaat8235.

[18] A. K. Jena, M. Ikegami, T. Miyasaka, *ACS Energy Lett.* **2017**, *2*, 1760.

[19] Z. Li, Z. Zhu, C.-C. Chueh, J. Luo, A. K.-Y. Jen, *Adv. Energy Mater.* **2016**, *6*, 1601165.

[20] R. S. Sanchez, E. Mas-Marza, *Sol. Energy Mater. Sol. Cells* **2016**, *158*, 189.

[21] C. T. Weisspfennig, M. M. Lee, J. Teuscher, P. Docampo, S. D. Stranks, H. J. Joyce, H. Bergmann, I. Bruder, D. V. Kondratuk, M. B. Johnston, H. J. Snaith, L. M. Herz, *J. Phys. Chem. C* **2013**, *117*, 19850.

[22] N. Wijeyasinghe, A. Regoutz, F. Eisner, T. Du, L. Tsetseris, Y.-H. Lin, H. Faber, P. Pattanasattayavong, J. Li, F. Yan, M. A. McLachlan, D. J. Payne, M. Heeney, T. D. Anthopoulos, *Adv. Funct. Mater.* **2017**, *27*, 1701818.

[23] S. Ye, W. Sun, Y. Li, W. Yan, H. Peng, Z. Bian, Z. Liu, C. Huang, *Nano Lett.* **2015**, *15*, 3723.

[24] S. S. Reddy, K. Gunasekar, J. H. Heo, S. H. Im, C. S. Kim, D.-H. Kim, J. H. Moon, J.

Y. Lee, M. Song, S.-H. Jin, *Adv. Mater.* **2016**, *28*, 686.

[25] S. Zhang, M. Stolterfoht, A. Armin, Q. Lin, F. Zu, J. Sobus, H. Jin, N. Koch, P. Meredith, P. L. Burn, D. Neher, *ACS Appl. Mater. Interfaces* **2018**, *10*, 21681.

[26] Z. Yu, L. Sun, *Adv. Energy Mater.* **2015**, *5*, 1500213.

[27] W. S. Yang, J. H. Noh, N. J. Jeon, Y. C. Kim, S. Ryu, J. Seo, S. Il Seok, *Science* **2015**, *348*, 1234.

[28] Y. Zhang, M. Elawad, Z. Yu, X. Jiang, J. Lai, L. Sun, *RSC Adv.* **2016**, *6*, 108888.

[29] T. Gatti, F. Lamberti, P. Topolovsek, M. Abdu-Aguye, R. Sorrentino, L. Perino, M. Salerno, L. Girardi, C. Marega, G. A. Rizzi, M. A. Loi, A. Petrozza, E. Menna, *Sol. RRL* **2018**, *2*, 1800013.

[30] M. Ulfa, T. Zhu, F. Goubard, T. Pauporté, *J. Mater. Chem. A* **2018**, *6*, 13350.

[31] N. Yaghoobi Nia, F. Matteocci, L. Cina, A. Di Carlo, *ChemSusChem* **2017**, *10*, 3854.

[32] Y. Miyazawa, M. Ikegami, H.-W. Chen, T. Ohshima, M. Imaizumi, K. Hirose, T. Miyasaka, *iScience* **2018**, *2*, 148.

[33] C. J. Brabec, M. Heeney, I. McCulloch, J. Nelson, *Chem. Soc. Rev.* **2011**, *40*, 1185.

[34] S. Tiwari, W. Takashima, S. K. Balasubramanian, S. Miyajima, S. Nagamatsu, S. S. Pandey, R. Prakash, *Jpn. J. Appl. Phys.* **2014**, *53*, 021601.

[35] A. Gadisa, W. D. Oosterbaan, K. Vandewal, J.-C. Bolsée, S. Bertho, J. D'Haen, L. Lutsen, D. Vanderzande, J. V. Manca, *Adv. Funct. Mater.* **2009**, *19*, 3300.

[36] Z. Wu, A. Petzold, T. Henze, T. Thurn-Albrecht, R. H. Lohwasser, M. Sommer, M. Thelakkat, *Macromolecules* **2010**, *43*, 4646.

[37] F. Padinger, R. S. Rittberger, N. S. Sariciftci, *Adv. Funct. Mater.* **2003**, *13*, 85.

[38] Z. Zhang, L. Qu, G. Shi, *J. Mater. Chem.* **2003**, *13*, 2858.

[39] E. H. Jung, N. J. Jeon, E. Y. Park, C. S. Moon, T. J. Shin, T.-Y. Yang, J. H. Noh, J. Seo, *Nature* **2019**, *567*, 511.

[40] Y. Guo, C. Liu, K. Inoue, K. Harano, H. Tanaka, E. Nakamura, *J. Mater. Chem. A*

2014, *2*, 13827.

[41] S. N. Habisreutinger, N. K. Noel, H. J. Snaith, R. J. Nicholas, *Adv. Energy Mater.* **2017**, *7*, 1601079.

[42] M. Arafat Mahmud, N. Kumar Elumalai, M. Baishakhi Upama, D. Wang, F. Haque, M. Wright, K. Howe Chan, C. Xu, A. Uddin, *Phys. status solidi - Rapid Res. Lett.* **2016**, *10*, 882.

[43] M. Cai, V. T. Tiong, T. Hreid, J. Bell, H. Wang, *J. Mater. Chem. A* **2015**, *3*, 2784.

[44] A. Abate, T. Leijtens, S. Pathak, J. Teuscher, R. Avolio, M. E. Errico, J. Kirkpatrik, J. M. Ball, P. Docampo, I. McPherson, H. J. Snaith, *Phys. Chem. Chem. Phys.* **2013**, *15*, 2572.

[45] H. J. Snaith, M. Grätzel, *Appl. Phys. Lett.* **2006**, *89*, 262114.

[46] A. Dualeh, T. Moehl, N. Tétreault, J. Teuscher, P. Gao, M. K. Nazeeruddin, M. Grätzel, *ACS Nano* **2014**, *8*, 362.

[47] S. Wang, M. Sina, P. Parikh, T. Uekert, B. Shahbazian, A. Devaraj, Y. S. Meng, *Nano Lett.* **2016**, *16*, 5594.

[48] M. M. Tavakoli, W. Tress, J. V. Milić, D. Kubicki, L. Emsley, M. Grätzel, *Energy Environ. Sci.* **2018**, *11*, 3310.

[49] J. W. Jung, J.-S. Park, I. K. Han, Y. Lee, C. Park, W. Kwon, M. Park, *J. Mater. Chem. A* **2017**, *5*, 12158.

[50] T. M. Koh, S. Dharani, H. Li, R. R. Prabhakar, N. Mathews, A. C. Grimsdale, S. G. Mhaisalkar, *ChemSusChem* **2014**, *7*, 1909.

[51] N. Yaghoobi Nia, P. Farahani, H. Sabzyan, M. Zendehdel, M. Oftadeh, *Phys. Chem. Chem. Phys.* **2014**, *16*, 11481.

[52] M. Nasr-Esfahani, M. Zendehdel, N. Yaghoobi Nia, B. Jafari, M. Khosravi Babadi, *RSC Adv.* **2014**, *4*, 15961.

[53] D. Karimian, B. Yadollahi, M. Zendehdel, V. Mirkhani, *RSC Adv.* **2015**, *5*, 76875.

[54] J. Burschka, A. Dualeh, F. Kessler, E. Baranoff, N.-L. Cevey-Ha, C. Yi, M. K. Nazeeruddin, M. Grätzel, *J. Am. Chem. Soc.* **2011**, *133*, 18042.

[55] K. Neumann, M. Thelakkat, *RSC Adv.* **2014**, *4*, 43550.

[56] J. H. Noh, N. J. Jeon, Y. C. Choi, M. K. Nazeeruddin, M. Grätzel, S. Il Seok, *J. Mater. Chem. A* **2013**, *1*, 11842.

[57] N. Yaghoobi Nia, M. Méndez, A. di Carlo, E. Palomares, *Philos. Trans. R. Soc. A Math. Phys. Eng. Sci.* **2019**, *377*, 20180315.

[58] N. Yaghoobi Nia, M. Zendehdel, L. Cinà, F. Matteocci, A. Di Carlo, *J. Mater. Chem. A* **2018**, *6*, 659.

[59] B. Taheri, N. Yaghoobi Nia, A. Agresti, S. Pescetelli, C. Ciceroni, A. E. Del Rio Castillo, L. Cinà, S. Bellani, F. Bonaccorso, A. Di Carlo, *2D Mater.* **2018**, *5*, 045034.

[60] M. Saliba, T. Matsui, J.-Y. Seo, K. Domanski, J.-P. Correa-Baena, M. K. Nazeeruddin, S. M. Zakeeruddin, W. Tress, A. Abate, A. Hagfeldt, M. Grätzel, *Energy Environ. Sci.* **2016**, *9*, 1989.

[61] W. Chen, Y. Wu, Y. Yue, J. Liu, W. Zhang, X. Yang, H. Chen, E. Bi, I. Ashraful, M. Grätzel, L. Han, *Science* **2015**, *350*, 944.

[62] A. Abate, S. Paek, F. Giordano, J.-P. Correa-Baena, M. Saliba, P. Gao, T. Matsui, J. Ko, S. M. Zakeeruddin, K. H. Dahmen, A. Hagfeldt, M. Grätzel, M. K. Nazeeruddin, *Energy Environ. Sci.* **2015**, *8*, 2946.

[63] Y. Tian, I. G. Scheblykin, *J. Phys. Chem. Lett.* **2015**, *6*, 3466.

[64] P. J. Brown, D. S. Thomas, A. Köhler, J. S. Wilson, J.-S. Kim, C. M. Ramsdale, H. Sirringhaus, R. H. Friend, *Phys. Rev. B* **2003**, *67*, 064203.

[65] B. Xue, B. Vaughan, C.-H. Poh, K. B. Burke, L. Thomsen, A. Stapleton, X. Zhou, G. W. Bryant, W. Belcher, P. C. Dastoor, *J. Phys. Chem. C* **2010**, *114*, 15797.

[66] T. S. Ripolles, A. Guerrero, G. Garcia-Belmonte, *Appl. Phys. Lett.* **2013**, *103*, 243306.

[67] L. E. McNeil, R. H. French, *J. Appl. Phys.* **2001**, *89*, 283.

[68] G. Dupuis, M. Menu, *Appl. Phys. A* **2006**, *83*, 469.

[69] M. Zendehdel, M. H. Habibi, M. S. Hashemzadeh-Esfarjani, *Sep. Sci. Technol.* **2014**, *49*, DOI 10.1080/01496395.2014.945186.

[70] M. H. Habibi, M. Mardani, M. Habibi, M. Zendehdel, *J. Mater. Sci. Mater. Electron.* **2017**, *28*, 3789.

[71] A. A. B. Baloch, F. H. Alharbi, G. Grancini, M. I. Hossain, M. K. Nazeeruddin, N. Tabet, *J. Phys. Chem. C* **2018**, *122*, 26805.

[72] R. S. Sanchez, V. Gonzalez-Pedro, J.-W. Lee, N.-G. Park, Y. S. Kang, I. Mora-Sero, J. Bisquert, *J. Phys. Chem. Lett.* **2014**, *5*, 2357.

[73] G. Niu, W. Li, F. Meng, L. Wang, H. Dong, Y. Qiu, *J. Mater. Chem. A* **2014**, *2*, 705.

[74] Y. Zhao, X. Gu, Y. Qiang, *Thin Solid Films* **2012**, *520*, 2814.

[75] J. M. Marin-Beloqui, L. Lanzetta, E. Palomares, *Chem. Mater.* **2016**, *28*, 207.

[76] L. Zhang, Device Physics of Perovskite Solar Cells, Iowa State University, Digital Repository, **2017**.

[77] X. Zhu, D. Yang, R. Yang, B. Yang, Z. Yang, X. Ren, J. Zhang, J. Niu, J. Feng, S. (Frank) Liu, *Nanoscale* **2017**, *9*, 12316.

[78] R. H. Bube, *J. Appl. Phys.* **1962**, *33*, 1733.

[79] S. A. Moiz, I. A. Khan, W. A. Younis, K. S. Karimov, in *Conduct. Polym.*, InTech, **2016**.

[80] T.-H. Le, Y. Kim, H. Yoon, T.-H. Le, Y. Kim, H. Yoon, *Polymers (Basel).* **2017**, *9*, 150.

[81] M. Alsari, A. J. Pearson, J. T.-W. Wang, Z. Wang, A. Montisci, N. C. Greenham, H. J. Snaith, S. Lilliu, R. H. Friend, *Sci. Rep.* **2018**, *8*, 5977.

[82] S. Wheeler, D. Bryant, J. Troughton, T. Kirchartz, T. Watson, J. Nelson, J. R. Durrant, *J. Phys. Chem. C* **2017**, *121*, 13496.

[83] Y. Ma, J. Fan, C. Zhang, H. Li, W. Li, Y. Mai, *RSC Adv.* **2017**, *7*, 37654.

[84] T. Gatti, S. Casaluci, M. Prato, M. Salerno, F. Di Stasio, A. Ansaldo, E. Menna, A. Di Carlo, F. Bonaccorso, *Adv. Funct. Mater.* **2016**, *26*, 7443.

[85] A. L. Palma, F. Matteocci, A. Agresti, S. Pescetelli, E. Calabro, L. Vesce, S. Christiansen, M. Schmidt, A. Di Carlo, *IEEE J. Photovoltaics* **2017**, *7*, 1674.

Supporting Information

Doping Strategy for Efficient and Stable Triple Cation Hybrid Perovskite Solar Cells and Module Based on Poly(3-Hexylthiophene)[P3HT] Hole Transport Layer

Narges Yaghoobi Nia[1], Enrico Lamanna[1,‡], Mahmoud Zendehdel[1,2‡], Alessandro L. Palma[1], Francesca Zurlo[3], Luigi Angelo Castriotta[1], Aldo Di Carlo[1,4]*.*

[1] CHOSE. (Centre for Hybrid and Organic Solar Energy), University of Rome ‘‘Tor Vergata’’, via delPolitecnico 1, Rome 00133, Italy.

[2] K.S.R.I (Kimia Solar Research Institute), Kimia Solar Company, Kashan, 87137-45868, Iran.

[3] Department of Chemical Science and Technologies, University of Rome Tor Vergata, Via dellaRicercaScientifica 1, 00133 Rome, Italy.

[4] LASE - Laboratory for Advanced Solar Energy, National University of Science and Technology, NUST-MISiS, 119049 Leninskiyprosect 6. Moscow, Russia

AUTHOR INFORMATION

Corresponding Author

.*E-mail: YAGHOOBI.NIA@ing.uniroma2.it* E-mail:aldo.dicarlo@uniroma2.it

a) b)

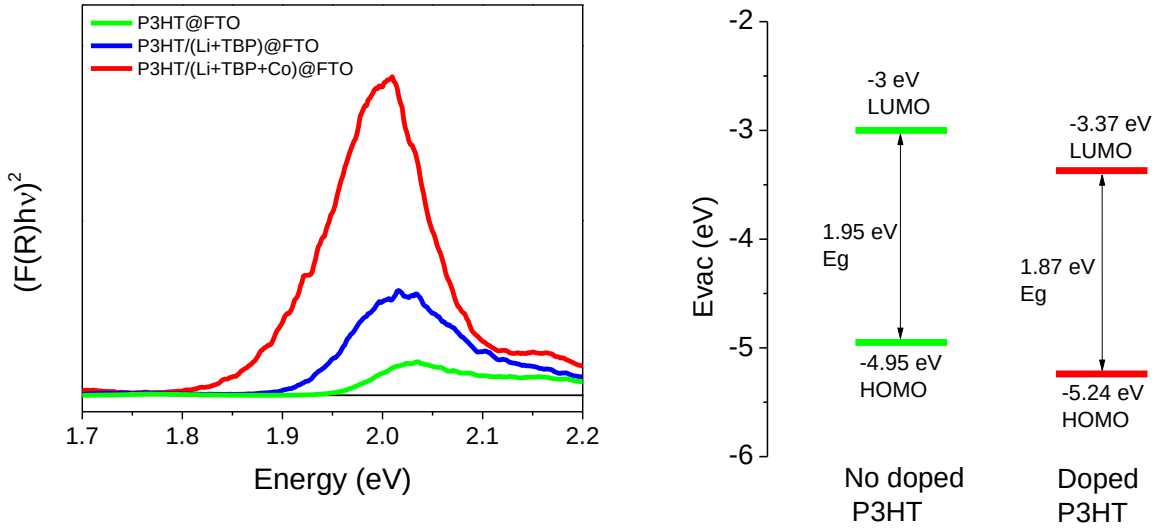

Fig. S1: a) Kubelka-Munk plots of the P3HT thin films coated on FTO substrate which are evaluated from DRS with representation of direct band gap. b) Energy diagram of P3HT layer at both doped and no-doped states.

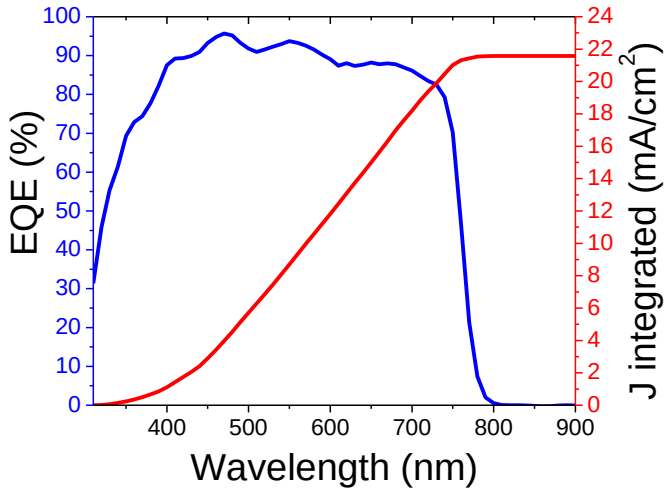

Fig S2: EQE curve of the champion small area device.

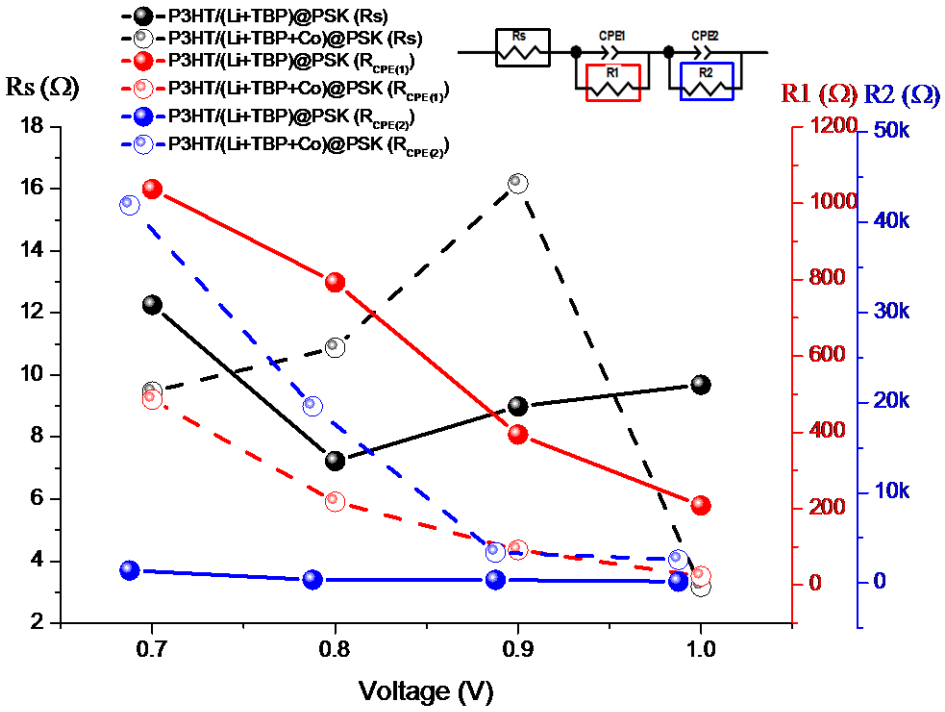

Fig. S3: Correlation between EIS fitted values of resistive elements and bias voltages.

a

)

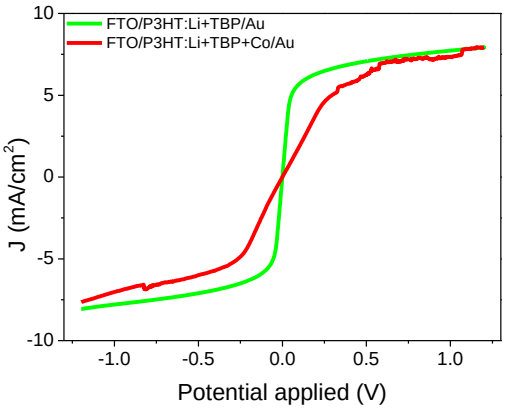

b)

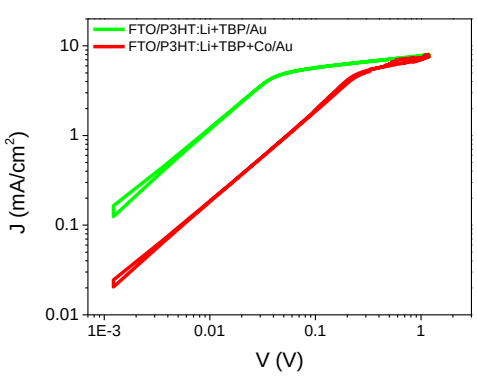

Fig. S4: a) JV curves of P3HT based diodes (P3HT layer without cobalt dopant compare to full doped (Li+TBP+Co) film sandwiched between FTO and Au electrodes) under dark condition. Bias potential sweep from -1.2 V to +1.2 V with scan rate of 50 mV/s. In order to evaluate the Space Charge-Limited Current behavior, the curves has been shown in logarithmic scale of both J and V (b).